[4] Humphrey, B. G., Jr., Panunzio, S., and Pinkus, O., "A Theoretical and Experimental Investigation of the Free-Piston Cycle," AFFDL-TR-66-204, Jan. 1967, Air Force Flight Dynamics Lab., Dayton, Ohio.

[5] Enkenhus, K. R. and Parazzoli, C., "The Longshot Free-Piston Cycle. Part I—Theory," VKI TN 51, Nov. 1968, von Kármán Institute for Fluid Dynamics, Rhode-Saint-Genèse, Belgium.

[6] Gaydon, A. G. and Hurle, I. R., *The Shock Tube in High-Temperature Chemical Physics*, Reinhold, New York, 1963.

[7] Stalker, R. J., "An Approximate Theory of Gun Tunnel Behaviour," *Journal of Fluid Mechanics*, Vol. 22, Pt. 4, 1965, pp. 657–670.

[8] Siegel, A. E., "The Theory of High-Speed Guns," AGARDograph 91, May 1965, NATO.

[9] Parazzoli, C. and Enkenhus, K. R., "The Longshot Free-Piston Cycle. Part II—Comparison of Theory with Experiment," VKI TN 52, Dec. 1968, von Kármán Institute for Fluid Dynamics, Rhode-Saint-Genèse, Belgium.

[10] Enkenhus, K. R., "On the Pressure Decay Rate in the Longshot Reservoir," VKI TN 40, 1967, von Kármán Institute for Fluid Dynamics, Rhode-Saint-Genèse, Belgium.

[11] Phinney, R., "Criterion for Vibrational Freezing in a Nozzle Expansion," *AIAA Journal*, Vol. 1, No. 2, Feb. 1963, pp. 496–497.

[12] Culotta, S. and Enkenhus, K. R., "Analytical Expressions for the Thermodynamic Properties of Dense Nitrogen," VKI TN 50, Dec. 1968, von Kármán Institute for Fluid Dynamics, Rhode-Saint-Genèse, Belgium.

[13] Grabau, M. and Brahinsky, H. S., "Thermodynamic Properties of Nitrogen from 300°K to 5000°K and from 1 to 1000 Amagats," AEDC-TR-66-69, Aug. 1966, Arnold Engineering Development Center.

[14] Culotta, S. and Richards, B. E., "Charts and Formulas for Determining Flow Conditions in Real Nitrogen Expanding Flows," VKI TN 58, Jan. 1970, von Kármán Institute for Fluid Dynamics, Rhode-Saint-Genèse, Belgium.

[15] Bailey, F. R., "Flat Plate Pressure Distribution and Heat Transfer in a Conical Hypersonic Flow," VKI TN 56, Jan. 1970, von Kármán Institute for Fluid Dynamics, Rhode-Saint-Genèse, Belgium.

JANUARY 1970 AIAA JOURNAL VOL. 8, NO. 1

Investigation of Supersonic Phenomena in a Two-Phase (Liquid-Gas) Tunnel

ROBERT B. EDDINGTON*
Air Force Institute of Technology, Wright-Patterson Air Force Base, Ohio

Homogeneous two-phase flows of dispersed liquid and gas having gas-to-liquid volume ratios around 1:1 exhibit the characteristics of a continuum flow with a greatly reduced sound propagational velocity. This velocity approaches 66 fps at atmospheric pressure for a homogeneous mixture of water and air, and reduces further as the square root of the static pressure. Flows of such mixtures at velocities in excess of the local velocity of sound can produce shock phenomena similar to that experienced in supersonic, gaseous media. A supersonic two-phase tunnel was designed and built to create normal and oblique shock structure that can be photographed and analyzed with a minimum of boundary-layer interference. The applicability of the isothermal continuum theory to such flows is confirmed empirically for volume ratios near 1:1. Auxiliary flow devices were constructed for the measurement of such difficult to determine flow parameters as the relative phase velocity, local void ratio, coefficient of friction, and stagnation pressure. A general change in the flow model matrix was found at volume ratios approaching 1:1. The coefficient of friction measured for supersonic flow was found to be a simple function of the local void ratio. Stagnation pressures measured for a wide range of flow conditions approximate an isentropic relation for a substantial part of the supersonic flow spectrum. Measurements of flow characteristics were made over a range of Mach numbers from 2.2 to 19.

Nomenclature

c = velocity of sound (fps)
M = Mach number
m = mass (slug/ft^3)
P = mixture pressure (lbf/ft^2)
P_3 = isentropic stagnation pressure, mixture (lbf/ft^2)
P_4 = normal shock plus isentropic stagnation pressure, mixture (lbf/ft^2)
r_m = gas-to-liquid mass ratio
r_v = gas-to-liquid volume ratio
u = X component of mixture velocity (fps)
$\bar{u}$ = component of mixture velocity normal to the shock wave (fps)
u' = component of mixture velocity parallel to inclined plane (fps)
v = downstream velocity component perpendicular to the upstream flow direction (fps)
$\mathcal{V}$ = volume (ft^3)
V = velocity (fps)
β = angle of shock wave with horizontal (deg)
θ = angle of inclined plane with the horizontal (deg)
ρ = mixture density (slug/ft^3)

Received January 31, 1969; revision received July 11, 1969. Portions of the results were presented as Paper 66-87 at the 3rd Aerospace Sciences Meeting, New York, January 24–26, 1966. The work was supported by the Jet Propulsion Laboratory of the California Institute of Technology. Technical monitors of the effort were D. G. Elliott of the Research and Advanced Concepts Section, Jet Propulsion Laboratory, and H. J. Stewart of the Department of Aeronautics, California Institute of Technology.

* Associate Professor of Mechanical Engineering; currently Staff Development Engineer, Directorate of Operational Requirements and Development Plans, DCS/R&D, HQ USAF, Washington, D. C.; Lt. Colonel U.S. Air Force.

τ_w = wall shear stress, mixture (lbf/ft²)
τ_{wl} = wall shear stress, liquid (lbf/ft²)
μ = micro

Subscripts

g = gas phase
l = liquid phase
1 = upstream of shock
2 = downstream of shock

1. Introduction and Approach to Isothermal Two-Phase Flow Relationships

FLOWS containing one or more distinguishable elements having both liquid and gaseous phases are generally known as "two-phase flows." To date, the majority of multiphase analytical and experimental investigations have been concerned with subsonic flows of space and time variable flow models. The formulation of the fundamental hydrodynamic equations for such systems can become very complex depending upon the extent to which phase and element interrelationships and position must be determined.

With the advent of high flow velocities and heat-transfer rates found in certain nuclear reactors, rocket propulsion systems and two-phase power generating equipment[1] time stable (in a broad sense) homogeneous bubble and homogeneous spray flows have appeared as principal characteristics of these systems. Such flows that have a volumetric ratio of gas-to-liquid between 0.1 and 10 and that are sufficiently homogeneous to be described as continuum flows can be treated by considerably simplified, hydrodynamical equations, particularly if the mixture is assumed to be isothermal.

One important aspect of two-phase continuum flows, however, which has received virtually no previous experimental study and little theoretical attention is the supersonic flow regime that may easily develop from the relatively low sonic velocity occurring within this range of void ratios. The major portion of this study is directed toward the examination and correlation with theory of the phenomena that is characteristic of supersonic, two-phase, nondissolving, liquid-gas flows.

Acoustic Propagation

The propagation of a pressure disturbance in a bubble-liquid mixture or froth was first investigated by Mallock.[2] Ackeret,[3] Wood,[4] and Spitzer[5] further derived relationships for the propagation and attenuation of oscillatory pressure disturbances in bubbly mixtures. Campbell[6] and Campbell and Pitcher[7] investigated the velocity and attenuation of single pressure pulses in bubbly mixtures.

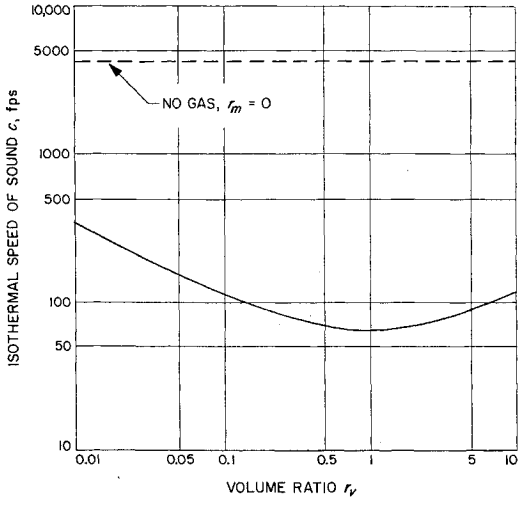

Fig. 1 Isothermal speed of sound in an air-water mixture at 530°R.

One general conclusion from these investigations is that a two-phase medium can be treated as an isothermal continuum for the propagation of acoustic waves, if the distance between bubble centers is less than $\frac{1}{2}$ wave length and if the bubble radii are less than 0.004 in., unless for sinusoidal oscillations, the sound frequency is less than 100 cps.[6] The sonic velocity c in the continuum depends upon the pressure P and the density ρ through the well-known ratio,

$$c = (dP/d\rho)^{1/2} \tag{1}$$

If the gas-to-liquid mass ratio is designated by r_m and the gas-to-liquid (static) volume ratio by r_v, then

$$r_m = \frac{m_g}{m_l} \text{ per unit volume}, \quad r_v = \frac{\mathcal{V}_g}{\mathcal{V}_l} \text{ per unit volume}$$

and the average density of the continuum can be written as

$$\rho = \rho_l[(1 + r_m)/(1 + r_v)] \tag{2}$$

where ρ_l is the liquid density.

For pressures less than 1000 psi, and bubble diameters in the vicinity of 0.004 in., the effects of compressibility and surface tension on a liquid such as water can be neglected. For volume ratios less than 10, the temperature changes in the continuum can be considered negligible so that, from Boyles' Law, the pressure times the volume is a constant that gives an isothermal equation of state;

$$P(r_v) = \text{const} \tag{3}$$

Combining Eqs. (2) and (3), and obtaining the derivatives of P and ρ as in Eq. (1), the velocity of sound in an isothermal continuum becomes

$$c = (1 + r_v)[P/\rho_l r_v(1 + r_m)]^{1/2} \tag{4}$$

The density of the gas can be ignored in formulation of Eq. (4) with an error in c of less than 0.5% over an r_v of 0.01 to 4.0.[6]

Figure (1) shows the isothermal speed of sound c in an air-water mixture as a function of r_v according to Eq. (4). A definite minimum can be seen for an $r_v = 1.0$ corresponding to $c = 65$ fps.

Based on Eq. (4), a Mach number can be defined in the usual form for the two-phase continuum flow as

$$M = \frac{V}{c} = \frac{V}{(1 + r_v)}\left[\frac{\rho_l r_v(1 + r_m)}{P}\right]^{1/2} \tag{5}$$

where the mixture velocity (V) is related to the phase velocities through the continuity equation for multiphase flow. For the range of volume ratios considered in this paper, the liquid velocity (V_l) can be used as the mixture velocity with

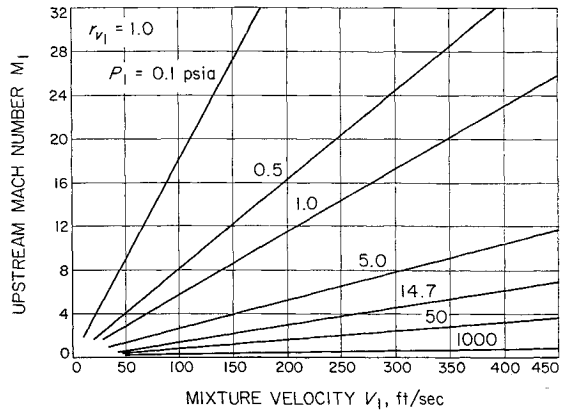

Fig. 2 Upstream Mach number as a function of mixture velocity for various values of static pressure ($0 \leq M_1 \leq 32$, $r_{v_1} = 1.0$).

Table 1 Two-phase tunnel dimensions and operating conditions

Upstream height	1.956 in.
Upstream width	0.756 in.
Upstream cross section	1.479 in.^{2}
Volume ratio (r_{v_1})	0.77–0.96
Test section height	1.600 in.
Test section width	0.381–0.756 in.
Test section length	4.00 in.
Water injection pressure	0–1000 psi
Water flow rate ($\dot{m}_l$)	0–100 lb/sec
Gas injection pressure	0–500 psi
Gas flow rate ($\dot{m}_g$)	0–0.36 lbm/sec
Mixture velocity (V_1)	0–334 fps
Mach number range (M_1)	$0 \simeq 100$
Reynolds number (maximum, based on tunnel height)	2×10^6
Power density	443 hp/in.^{2}

an error on the order of 0.1%. The relationship of Eq. (5) is plotted parametrically in Fig. 2 for a volume ratio of 1.0.

Considerations for Shock Wave Propagation

Parkin et al.[8] extended the analysis of Campbell and Pitcher[7] to far more intense shock waves. Such interphase relationships as surface tension, dynamic bubble behavior, heat conduction, and gas phase dissolution were considered. The results of their analysis suggest that for a range of downstream pressures up to 10,000 psia and over, a range of volume ratios from 0.1 to 10, the two-phase flow can be considered isothermal through normal shock structure. Further, the most important flow parameters such as pressure, velocity, density, and volume ratio can be derived directly from the conservation relations of mass and momentum and the isothermal equation of state applied to both sides of the shock structure, ignoring the relaxation processes within. The experimental work reported in the following sections will demonstrate how well this approach approximates the flow characteristics over a wide range of shock strengths.

2. Supersonic Two-Phase Tunnel

Indications of normal shock phenomena had been reported in previous diffuser studies.[9] However, since no previous investigations into the completely supersonic regime of two-phase flow had been performed, such flow characteristics as boundary-layer buildup, shock thickness, shock visibility, flow stability, and total head pressure were uncertain. In order to determine, experimentally, the possible existence of normal and oblique shock waves in two-phase flow and make measurements of the significant flow characteristics, a tunnel with unusual flexibility was required.

Utilizing a water pump in the hydrodynamics laboratory at the Caltech Jet Propulsion Laboratory having an output capacity of 720 gal/min at 1100 psi, a tunnel was designed with a $1\frac{1}{2}$ in.^{2} test section capable of attaining a Mach number of 5.0 at atmospheric pressure and Mach numbers approaching 100 near the vapor pressure of water at ambient temperature. Figure 3 shows a line sketch of the tunnel assembly depicting the relative positions of the major tunnel components. The high-pressure water enters the calming duct at the left. The two-phase injector consists of a bundle of 192 small (0.70 in. i.d.) stainless steel tubes through which the high-pressure water is accelerated in excess of 300 fps and about which nitrogen gas is injected to form a high-velocity, low-pressure two-phase mixture in the rectangular mixing duct. Transparent, movable sidewall, and boundary-layer knife assemblies in the test section allow removal of the side boundary layers which have built up in the low-pressure mixing section. The top and bottom boundary layers are removed by fixed knife assemblies set downstream from the

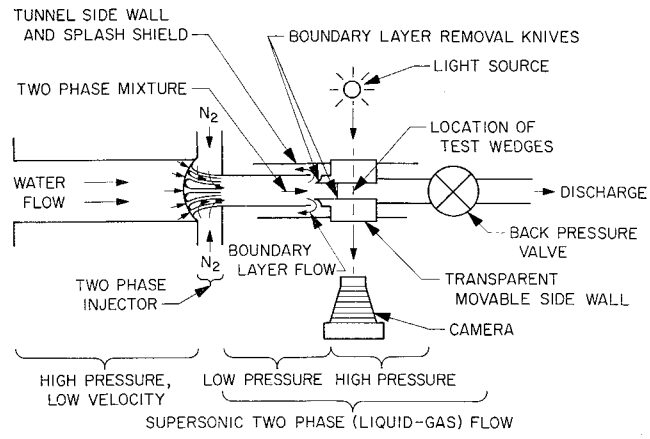

Fig. 3 Schematic of two-phase tunnel and photographic equipment.

sidewall knives at a position which can be viewed through the transparent sidewalls. The fixed assemblies serve as a convenient holding point for a normal shock, when the test section discharge is constricted by the back pressure valve in the discharge duct. The high-velocity boundary-layer flow is contained by outer tunnel walls and returned to the main water sump through a discharge duct in the bottom of the test section.

A substitute lower knife assembly also serves as a model support as shown in Fig. 4. A total head probe housing is attached to the upper boundary-layer knife. Sealing glands at the top of the housing allow three-dimensional positioning of the probe through normal shock structure at pressures ranging to 1000 psi. Static pressure is measured through pressure taps drilled along the center line of the opposite plexiglass sidewall as seen in the background of this figure. The assembled tunnel with the outer splash shields and protective glass cover window is shown in Fig. 5. Table 1 lists the significant tunnel dimensions and operating parameters.

3. Calibration of the Tunnel and Determination of the Two-Phase Flow Model

Tunnel Calibration

Determination of the Mach number in the tunnel test section is dependent upon an accurate knowledge of the liquid velocity, gas velocity, and local volume ratio. Since instrumentation is not available for measurement of such two-phase characteristics, a duplicate tunnel was constructed containing the variable side boundary-layer knives and terminating at the position of the fixed boundary-layer knives. Ducts were attached to all boundary-layer slots so that the individual liquid mass flow rates could be measured. The tunnel assembly was placed on a thrust stand allowing measurement of the thrust from the resultant core flow in

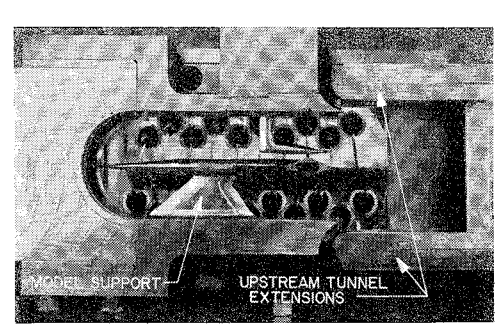

Fig. 4 Closeup of test section showing typical model placement and forward duct extensions.

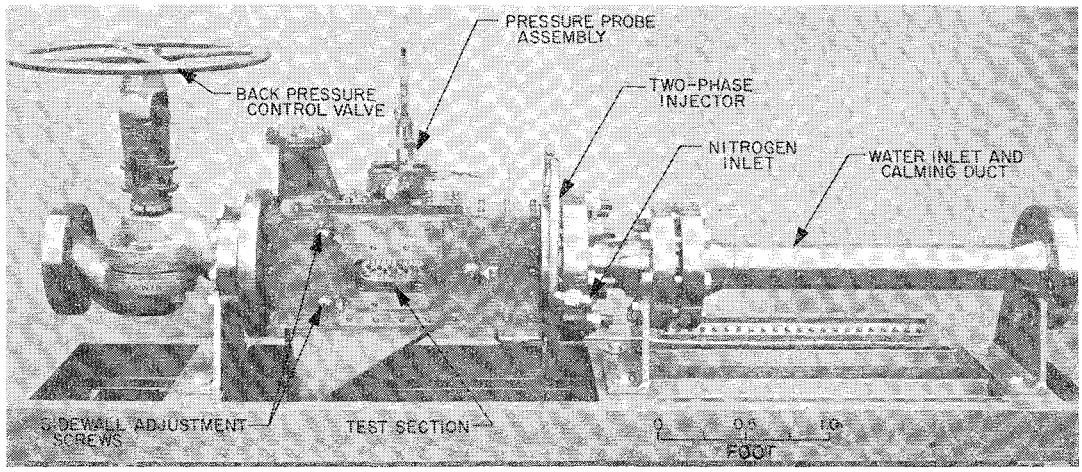

Fig. 5 Side view of complete tunnel assembly.

the test section at various mass flow rates and side boundary-layer knife settings.

From a simple force balance relationship values of the average liquid core velocity (V_{l_1}) were determined for the full range of liquid and gas mass flow rates used in all later tunnel testing. With the liquid velocity and mass flow rate in the core known, the continuity relation gives the liquid core area which combined with the known cross sectional area between the knives gives the local gas area and gas-to-liquid volume ratio. By repeating all measurements at increments of boundary-layer thickness from the wall to the core, the liquid velocity profiles, local volume ratios, and gas-liquid distributions in the boundary layer were determined. Measurements of the gas mass flow rates along with the continuity relationship and the computed local gas cross sectional areas then gave the gas velocity in the core.

Plots of the local liquid velocity vs distance from the sidewall are shown in Fig. 6. The curves approach zero slope at a depth of approximately 0.150 in. from the sidewall. Consequently, all measurements of the supersonic phenomena to be reported in subsequent sections are made with $\cong$0.150 in. of the boundary layer removed.

Flow Model

The liquid velocity was found to exceed the gas velocity by 17 to 20% regardless of the gas-to-liquid mass ratio. This condition suggested the existence of a slight positive pressure gradient in the mixing duct which was confirmed by

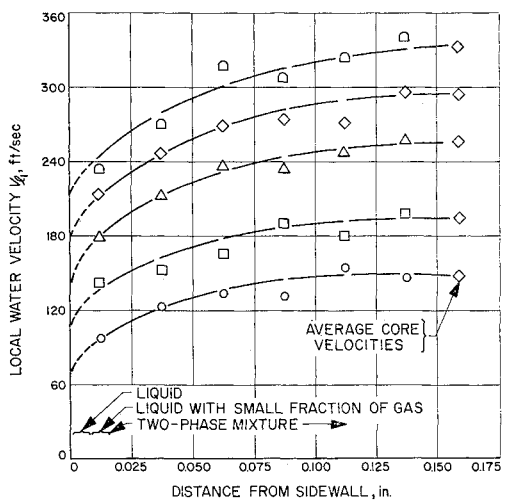

Fig. 6 Liquid velocity profiles, 8.5 in. downstream from the injector face.

static pressure measurements along the length of the duct. For a relatively immiscible mixture such as nitrogen and water in which there is negligible mass transfer between phases and a mass ratio of the order 10^{-3}, a static pressure gradient is primarily sustained by the drag between phases. With relative phase velocity and static pressure gradient information comparisons could be made with possible geometric liquid-gas distribution models.

Three models were chosen, individual water streams in gas, a water droplet distribution in gas, and a gas bubble distribution in water. The liquid stream drag model was found to correspond to a pressure gradient of an order 100 times less than measured, whereas the gas bubble in water corresponded to a pressure gradient 1000 to 10,000 times greater than measured. The water droplet model corresponded to a pressure gradient that was within a factor of 10 of that measured.

High-speed ($\frac{1}{2}\mu$ sec) still pictures of the two-phase flow revealed a bubble structure of two basic size groups in a water matrix. However, the bubbles were formed into chain-like groups oriented parallel with the flow. With increasing flow velocities, the size of the groups tended to decrease.

Although at the extremes of volume ratio for homogeneous flow of 0.1 and 10, one may reasonably expect geometric distributions of bubble in liquid and liquid droplet in gas, respectively, in the vicinity of a volume ratio of 1 to 1 no such simple distribution exists. The chain-like arrangement apparently reduces drag on the gas bubbles by three orders of magnitude. At a distance much further from the injector it is quite possible that the bubbles would tend to separate. Additional evidence relating to the nature of the upstream gas-liquid structure is provided in the discussion of normal shock structure.

4. Normal Shocks

Fundamentals

As previously stated, for a relatively nondissolving mixture such as air or nitrogen and water at mass ratios between 0.1 and 10, the coupling of heat, mass, and momentum transfer between phases can be neglected in the energy and momentum equations with negligible error. Further, the flow can be considered isothermal through normal shock structure and the relationships for the most important flow parameters can be derived directly from the conservation relations of mass and momentum and the isothermal equation of state.

Let subscript 1 denote the region ahead of the shock and subscript 2, the region behind the shock. The continuity

equation across the normal shock is

$$\rho_1 V_1 = \rho_2 V_2 \tag{6}$$

and the momentum equation is

$$\rho_1 V_1^2 - \rho_2 V_2^2 = P_2 - P_1 \tag{7}$$

Combining Eqs. (6) and (7), and employing Eqs. (2) and (3) on both sides of the shock and noting in addition that $r_{m_1} = r_{m_2}$ from a control volume analysis, the pressure downstream of the shock is

$$P_2 = \frac{\rho_l V_1^2 r_{v_1}(1 + r_{m_1})}{(1 + r_{v_1})^2} \tag{8}$$

Comparing Eqs. (8) and (4), the pressure ratio becomes a function of the upstream Mach number,

$$P_2/P_1 = M_1^2 \tag{9}$$

Combining Eqs. (3) and (9), the downstream volume ratio is

$$r_{v_2} = r_{v_1}/M_1^2 \tag{10}$$

Combining Eqs. (7) and (10) with the ratio of average stream densities in terms of mass and volume ratios at the two stations gives the downstream velocity relation as

$$V_2 = \frac{V_1}{M_1^2}\left(\frac{M_1^2 + r_{v_1}}{1 + r_{v_1}}\right) \tag{11}$$

By definition, the downstream Mach number is

$$M_2 = V_2/c_2 \tag{12}$$

which, with Eq. (4) for c_2, leaves

$$M_2 = \frac{V_2}{(1 + r_{v_2})}\left[\frac{\rho_l r_{v_2}(1 + r_{m_2})}{P_2}\right]^{1/2} \tag{13}$$

Substituting Eq. (11) for V_2 and combining with Eq. (4) the downstream Mach number relation becomes

$$M_2 M_1 = 1 \tag{14}$$

Results

During operation of the tunnel, it was found that restriction of the flow by the back pressure valve would readily create a stable, normal shock on the leading edge of the upper and lower boundary-layer knives in the test section. The static pressure taps, separated by 0.2 in. along the center line, provided static pressure sampling through the depth of the shock structure and the three axis probe provided both total head and static pressure surveys through the depth, width, and height of the shock structure.

With maximum boundary-layer removal, the normal shock phenomena appeared as two black lines approximately 0.10 in. apart. The two lines tend to merge into one because the camera lens was not coincident with the shock center line,

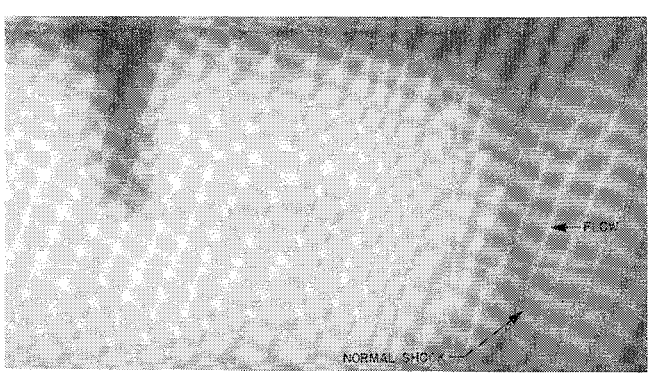

Fig. 7 Normal shock $M_1 = 3.95$.

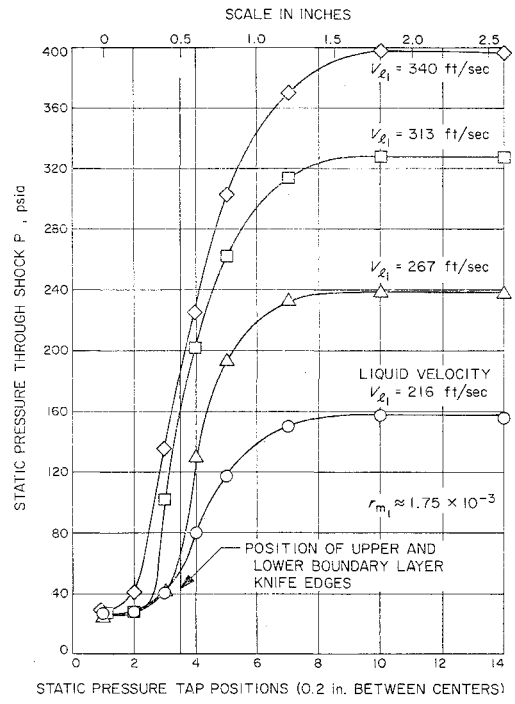

Fig. 8 Static pressure as a function of horizontal position through a normal shock for values of liquid velocity (V_{l_1}).

(Fig. 7). As the width of the test section was increased, the depth of the observable shock phenomena increased to a maximum of $\cong$1.0 in. (Ref. 11).

The time required for the collapse of a 0.010 in. diam bubble at 200 fps is about 10^{-5} sec which is approximately the time required for the mixture to travel 0.05 in. The time required to reach 90% of thermo-dynamic equilibrium is approximately 1 msec which is the time required to travel 1 in. at the downstream velocity.

The initial dark line is apparently the result of the turbulence of bubble compression; the light area, a nearly liquid region in which the bubbles have reached their minimum size and the following dark line, the bubble rebound and turbulence region. This is followed by a transition region leading to thermo-dynamic equilibrium as evidenced by a gradual increase in light transmission as bubble size again decreases along with turbulence.

Static pressure profiles across the shock structure were continuous as expected, since static pressure gradients can be sustained only by the drag between the phases for the conditions specified. Upstream, the bubbles are arranged in chains with a relatively low average coefficient of drag (C_d). The entrance of these chains into the shock front compresses the bubbles and destroys their connecting chain structure increasing their effective average C_d. The static pressure gradient is then indicative of the average C_d change within the shock structure. After reaching a maximum C_d configuration, the pressure gradient should decrease with pressure and approach its downstream value asymptotically as the bubble size is established by thermal equilibrium.

Static pressure plots at various Mach numbers and liquid velocities confirm this hypothesis. A plot of static pressure as a function of horizontal position through a normal shock for values of liquid velocity is shown in Fig. 8. At the lower velocity, the profile reaches upstream with a gentle gradient while at the higher velocities, the leading foot of the profiles is shortened and the gradients reach very large values.

Correlation of the pressure profile curves with the first visual evidence of a change in the upstream flow pattern as it approaches the shock position, indicates that changes in visual density, bubble size, and bubble orientation occur

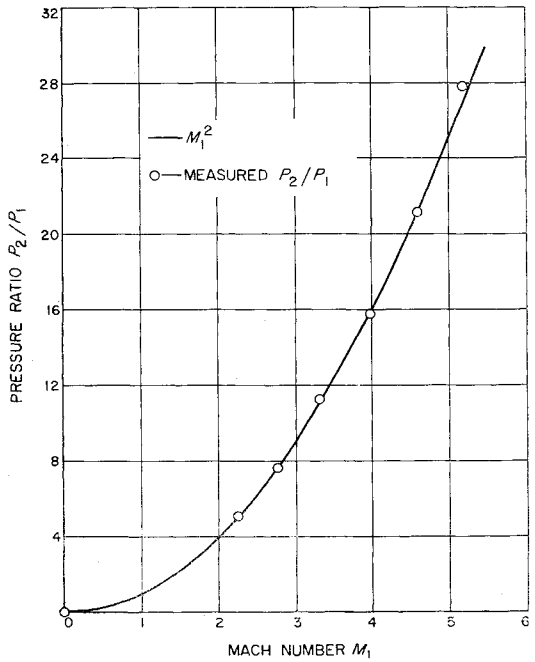

Fig. 9 Pressure ratio as a function of Mach number for a normal shock.

simultaneously with the relatively rapid increase in pressure gradient for a nearly constant volume ratio equal to 0.77. Reduction of the gas-to-liquid mass ratio at all velocities tends to steepen the maximum pressure gradient as expected from the better distribution of bubbles upon compression.

Static Pressure Ratio

According to Eq. (9), the static pressure ratio across a normal shock is proportional to the square of the Mach number. Because Mach number includes V, r_v and r_m, the validity of this simple proportionality supplies strong confirmation of the basic isothermal relations developed through Eq. (14) and the parameters of actual tunnel operation. A plot of the measured static pressure ratio vs the isothermal theory is shown in Fig. 9. The results of the plot fall within 2% of the theory through the full range of tunnel velocities and Mach numbers up through $M_1 = 6$.

The downstream static pressure was found to be essentially independent of the upstream static pressure for pressures $P_1 < 50$ psia. Parametric plots of Eq. (8) show that the effect of an r_m increase with pressure becomes significant for $P_1 > 100$ psia.[11]

The downstream mixture velocity cannot be measured conveniently in a thrust arrangement as was done for the upstream velocity. However, sufficient movement of bubble strata occurred downstream of the normal shock to permit mixture velocity determination from analysis of high-speed (26,000 frames/sec) Dynafax sequences. A plot of the measured values of downstream-to-upstream velocity ratio (V_2/V_1) as a function of Mach number is shown in Fig. 10. The data agrees within 10% of the isothermal theory up to $M_1 = 12$. Because the strata observed in the flow consists primarily of gas voids, it will be somewhat slower than the average liquid velocity (V_{l_2}) and since it is necessarily close to the wall, it will be further slowed in the development of a wall boundary layer, which is evident in the results plotted.

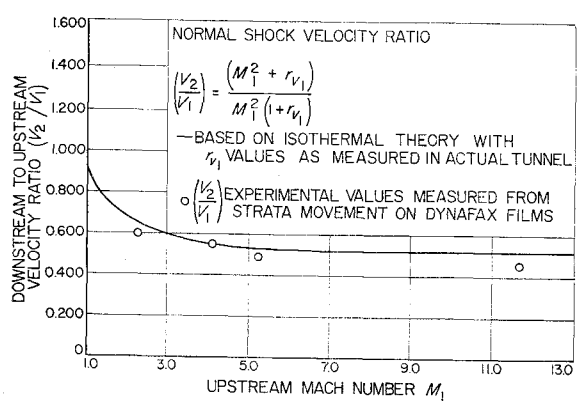

Fig. 10 Velocity ratio as a function of upstream Mach number at actual tunnel r_{v_1} values.

5. Oblique Shocks

Fundamentals

The normal shock analysis can be expanded to oblique shock waves with relative ease for the isothermal case by using the geometrical relationships common to the derivation of oblique shock relations for gaseous single-phase media. The equations of continuity and momentum, mixture density and velocity, the isothermal equation and the geometrical relationships form a complete set of equations for the determination of the downstream flow characteristics.

With reference to Fig. 11, the continuity equation can be written as

$$\rho_1 u_1 \sin\beta = \rho_2(u_2 \sin\beta - v_2 \cos\beta) \tag{15}$$

The momentum equations normal and parallel to the shock wave are
normal

$$P_1 + \rho_1 u_1^2 \sin^2\beta = P_2 + \rho_2(u_2 \sin\beta - v_2 \cos\beta)^2 \tag{16}$$

parallel

$$\rho_1 u_1^2 \sin\beta \cos\beta = \rho_2(u_2 \sin\beta - v_2 \cos\beta) \times (u_2 \cos\beta + v_2 \sin\beta) \tag{17}$$

Combining these relationships with the isothermal equation of state, mixture density, and Mach number, each written for both upstream and downstream parameters, the various significant quantities of the oblique shock and downstream conditions can be derived as a function of the upstream conditions and boundary constraints. The shock angle β cannot be explicitedly solved for and appears with Mach number M_1, volume ratio r_{v_1}, and deflection angle θ as

$$\frac{1}{M_1^2} = \frac{(-\sin^3\beta \sin\theta) + r_{v_1}(\sin^2\beta \cos\beta \cos\theta) - (\sin\beta \cos^2\beta \sin\theta)(1 + r_{v_1})}{r_{v_1}[\cos(\beta - \theta)]} \tag{18}$$

The pressure ratio in terms of upstream Mach number and shock angle is

$$P_2/P_1 = M_1^2 \sin^2\beta \tag{19}$$

and the ratio of volume ratios is

$$r_{v_2}/r_{v_1} = (M_1^2 \sin^2\beta)^{-1} \tag{20}$$

The downstream Mach number can be obtained as a function of the shock and deflection angles, the upstream Mach

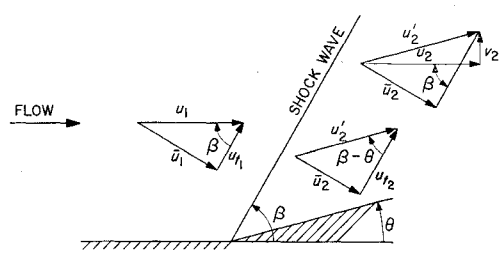

Fig. 11 Oblique shock relationships.

number, and the upstream volume ratio as

$$M_2 = \frac{M_1(1 + r_{v_1})}{(\cos\theta + \tan\beta \sin\theta)(M_1^2 \sin^2\beta + r_{v_1})} \quad (21)$$

Equations (18–21) are sufficient to describe the downstream flow and the shock geometry for any initial values of upstream Mach number, volume ratio, pressure, and flow deflection angle. The foregoing derivation is somewhat idealized, however, since a portion of the deflection geometry will necessarily involve incomplete relaxation processes depending upon the proximity of the shock wave to the deflecting surface.

Shock Angle β

Equation (18) cannot be solved for shock angle β and, consequently, solutions of β for initial values of deflection angle θ, M_1, and r_{v_1} must be solved by iteration on a digital computer. The results of such computations show that an increase in r_{v_1} increases the maximum θ for which an oblique shock attachment can occur, while simultaneously decreasing the shock angle β for any fixed value of M_1 and θ. Further, β is a strong function of Mach number near the limiting minimum Mach number, decreasing to a lower limit near $M_1 = 20$. Beyond $M_1 = 20$, β becomes nearly constant.[11]

Experimental determination of oblique shock angles was accomplished with double wedge models mounted on the lower boundary-layer knife. The leading edge of the model was located on the center line of the test section as previously shown in Fig. 4. The wedges are 0.5 in. wide and when placed symmetrically within the test section, allow removal of 0.127 in. of boundary layer on each side. The sidewall velocity at this depth would be within 2% of the core velocity.

Wedges of 4°, 10°, and 20° deflection were subjected to supersonic, two-phase flows ranging in Mach number M_1 from 1 to 20. Because the Mach number is a function of both mixture velocity and pressure, test series were made with runs at constant pressure and various velocities and runs at constant velocity and various pressures to determine the behavior of such oblique shock characteristics as shock angle and downstream pressure with Mach number.

Figure 12 shows the variation of β as a function of Mach number M_1 for flow deflections of 4° and 10°. Some interaction between the wedge shock and the top and bottom of the tunnel walls was visibly evident at the lower Mach numbers, suggesting that the test section choked near a Mach number of ≅2.2. The experimental data points between $M_1 = 2.2$ and 2.7 on Fig. 12, for the 10° wedge, confirm the sharp upturn of the theoretical curve in this region and the ultimate disattachment of the oblique shock at Mach numbers less than 2.2. The data accumulated at Mach numbers

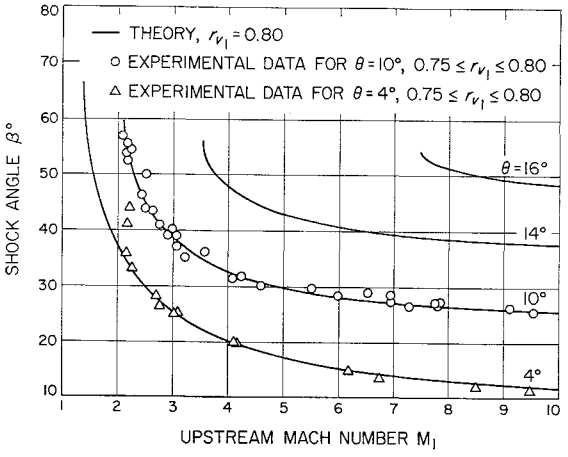

Fig. 12 Measured values of shock angle as a function of Mach number for 4° and 10° deflection wedges.

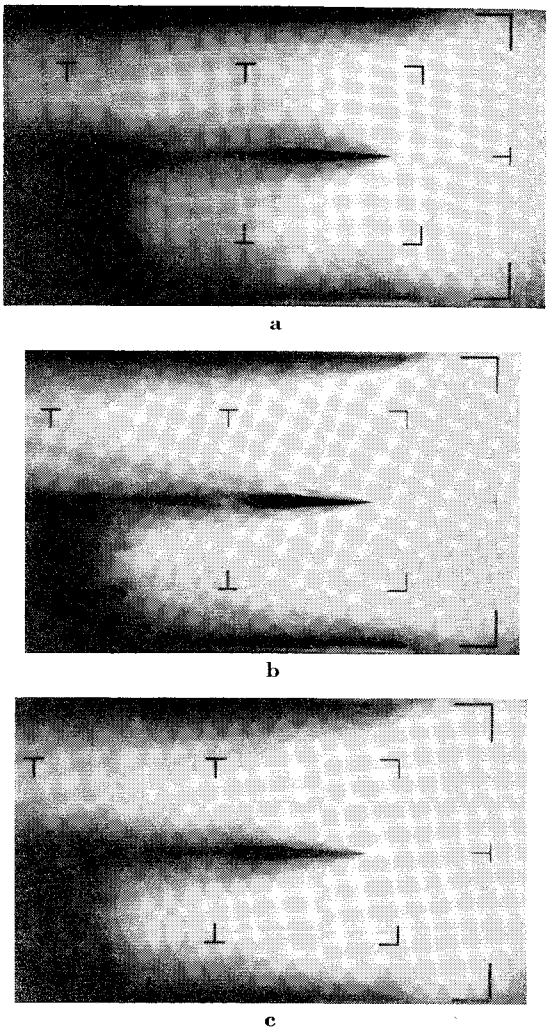

Fig. 13 Infrared photographs of supersonic, two-phase flow over a 4° deflection wedge at various Mach numbers a) $M_1 = 2.25$, b) $M_1 = 4.20$, c) $M_1 = 10.5$.

between 10 and 20 closely substantiate the validity of the asymptotic nature of the theoretical curves to a constant value in the upper Mach number ranges.[11]

Figures 13a–13c show a sequence of increasing Mach numbers for the 4° deflection wedge and Figs. 14a–14c, a similar sequence for the 10° wedge. The oblique shocks from the leading edge of the 10° wedge are more clearly defined than those from the 4° deflection wedge. A complete void exists behind the wedges up to nearly $M_1 = 4.0$. At higher liquid velocities, the pressure is sufficiently high behind the shock to turn the flow more quickly and partially close the void area. There are no expansion structures evident in the two-phase flow that are capable of turning the flow about a sharp corner.

Static Pressure Ratio

Figure 15 shows pressure ratio P_2/P_1 as a function of Mach number for flow deflections θ of 4° and 10° at an $r_{v_1} = 0.8$ which corresponds to a flow velocity of 180 fps. The experimental data conforms closely to the isothermal theory at the specific values of r_{v_1} plotted. Generally, at the lower liquid velocities, a very close approximation of the experimental data to the isothermal theory is observed. At the higher liquid velocities and at Mach numbers (M_1) exceeding 4.2, the experimental pressure ratio tends to exceed the isothermal theory. The scatter in this region is sufficiently great, however, to make the suggestion of a firm trend questionable.

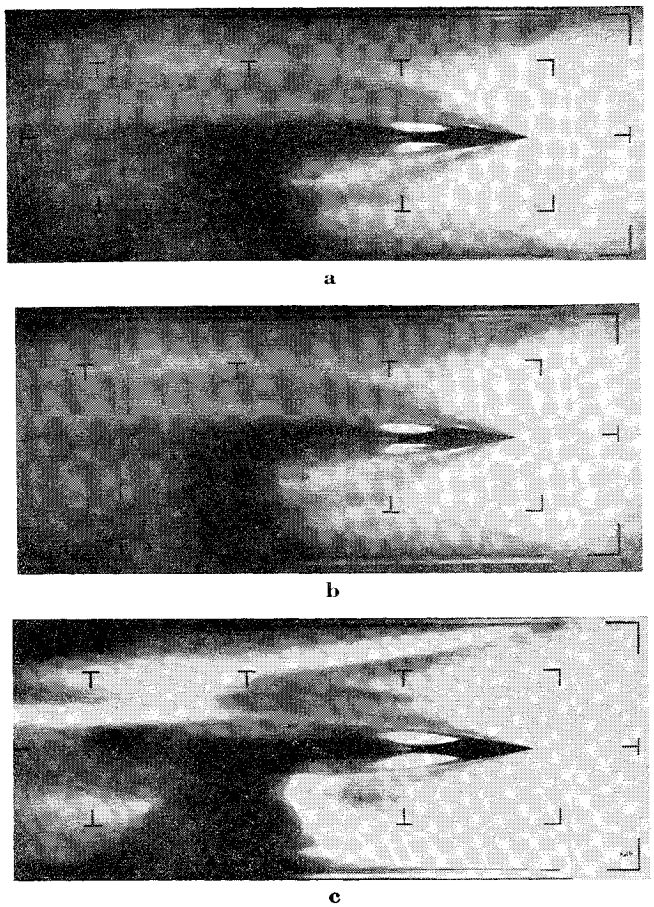

Fig. 14 Infrared photographs of supersonic, two-phase flow over a 10° deflection wedge at various Mach numbers a) $M_1 = 2.40$, b) $M_1 = 4.95$, c) $M_1 = 13.0$.

The downstream Mach number M_2 in Eq. (21) is a function of four variables M_1, r_{v1}, β, and θ which have the relationship given in Eq. (18). By constraining the four variables through this equation, the values of downstream Mach number can be determined from Eq. (21). A plot of M_2 as a function of M_1 for values of θ is shown in Fig. 16.

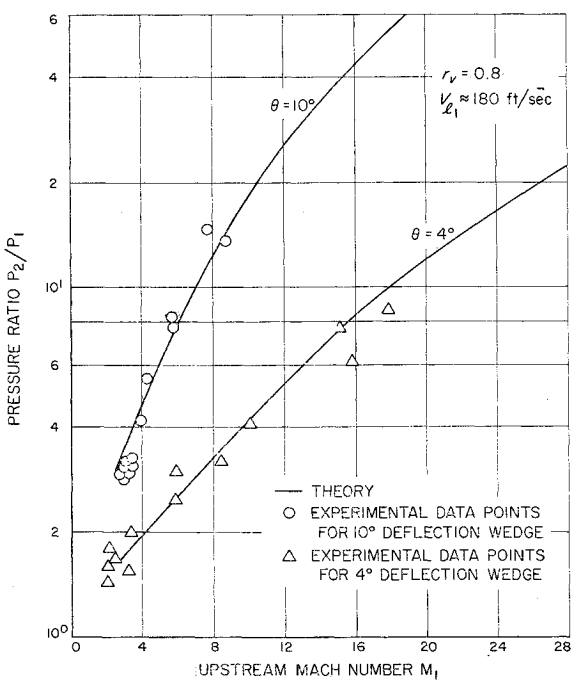

Fig. 15 Oblique shock pressure ratio as a function of Mach number for 4° and 10° deflection wedges.

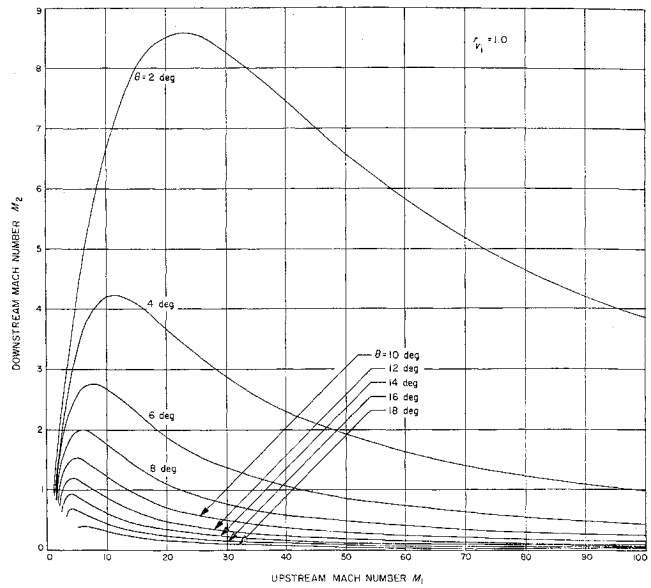

Fig. 16 Oblique shock downstream Mach number as a function of the upstream Mach number for values of deflection angle ($r_{v1} = 1.0$).

Considering that Pr_v = const, the downstream volume ratio r_{v2} is inversely proportional to the downstream pressure for various values of deflection angle θ. Experimental data was not obtainable for comparison.

Limiting Deflection Angle for Oblique Shock Attachment

Envelopes of applicability for deflection angle θ as a function of Mach number M_1 according to Eq. (18) are shown in Ref. 11. Limiting values of θ exist for each value of Mach number M_1 beyond which the shock wave will become unattached and the oblique shock relations will cease to apply. Confirmation of the sensitivity of the oblique shock formation to the limiting deflection angle has been experimentally confirmed with a 20° deflection wedge. The maximum deflection angle according to Eq. (18) in a flow with an $r_{v1} = 0.96$ and $M_1 = 4.0$ is approximately 17°.

Figure 17 shows a flow at $M_1 = 4.0$ over a 20° wedge at an exposure of $\frac{1}{2}$ μsec. The shock wave appears close to attachment, yet there is an obvious rounding in front of the leading edge. To investigate the leading edge phenomena more thoroughly, isodensity analyses were made of the negatives of this flow condition. Regions of distinct density variation associated with shock phenomena were evident ahead of the leading edge. Measurements of the angles of the leading shock structure near $M_1 = 4.0$ from various photographs indicate that the basic shock angle β lies between 53° and 57°. The limiting β for $\theta = 17°$ at $M_1 = 4.0$ is 57°. At higher Mach numbers, the measured angle of β for the 20° deflection wedge remained near 57°. Thus, the relatively constant value of shock angle β and the evidence of shock structure well ahead of the leading edge confirm the nonattachment of the shock structure at a deflection angle θ slightly in excess of the limiting angle for oblique shock attachment.

6. Stagnation Pressure Recovery

Stagnation pressure surveys were made with a total head probe at positions both upstream and downstream from normal shock structure and over the full range of flow conditions used in the tunnel. It was found that the results for supersonic two-phase liquid-gas flows could be reasonably bounded by a prediction of the isentropic stagnation pressure recovery

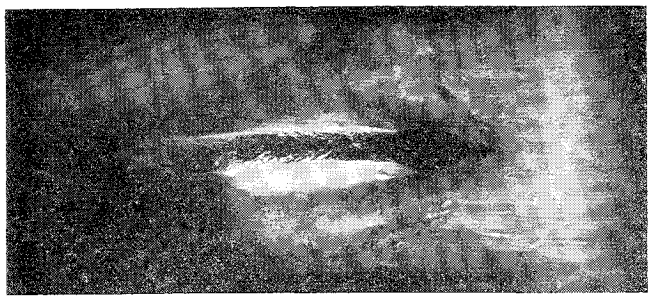

Fig. 17 One half μsec exposure of supersonic flow over a 20° deflection wedge at Mach number (M_1 = 4.0).

for the upper bound and a prediction of the normal shock plus isentropic stagnation pressure recovery for the lower bound within the Mach number range of the tests.

The isentropic stagnation pressure for homogeneous two-phase liquid-gas flows considered in this paper can be developed by assuming that the mixture can decelerate over a finite distance with a change in cross-sectional area. The momentum equation at each point is then

$$\rho V dV = -dP \tag{22}$$

This equation can be integrated with the aid of Eqs. (2) and (3) to give

$$P_2 = P_1 + \frac{1}{2}\rho_l(1 + r_{m_1})(V_1^2 - V_2^2) - r_{v_1}P_1 \ln\left(\frac{P_2}{P_1}\right) \tag{23}$$

To distinguish this pressure from the downstream pressure of normal shock flow, stagnation pressure recovery is designated P_3. The normal shock plus isentropic stagnation pressure can be derived similarly with the aid of Eq. (8) and is designated P_4.

The measured stagnation pressure as a function of liquid velocity (V_1) along with the theoretical isentropic stagnation pressure recovery and normal shock plus isentropic recovery curves is shown in Fig. 18. The probe pressure data closely follows the isentropic theory up to a liquid velocity of about 270 fps and falls away to 10% lower than the theoretical value at a velocity of 335 fps. In comparison with the normal shock plus isentropic stagnation pressure recovery, the measured values are generally in excess of the theory by about 9%. The measured values of stagnation pressure downstream of a normal shock lie about 4% above the theory for liquid velocities up to 200 fps, and at the higher velocity of 335 fps, approach to within a few percent of the latter theory.

7. Determination of Wall Shear in Two-Phase Flow

Wall shear (τ_w), or coefficient of friction (C_f), can be determined, if accurate measurements of thrust, static pressure, and gas and liquid flow rates can be made for different known lengths of the flow duct. The two-phase injector described previously was attached to a duct 15 in. in length and 0.75 × 1.95 in. in cross section and the assembly mounted on a thrust stand. Sections of duct approximately 2 in. long were removed between thrust measurements for a determination of wall shear.

By computing τ_{w_l} to correspond with a completely liquid-filled duct at the same velocity as the two-phase mixture, the ratio of shear stresses (τ_w/τ_{w_l}) was determined for each velocity and plotted as a function of liquid volume fraction for the two groups of data. From a previous but less accurate experiment of this type, wall shear results corresponding to a liquid volume fraction of 0.35 were available. Both groups of results are shown in Fig. 19. Comparison with a straight line between zero (wall shear with a pure gas would be 0.0013

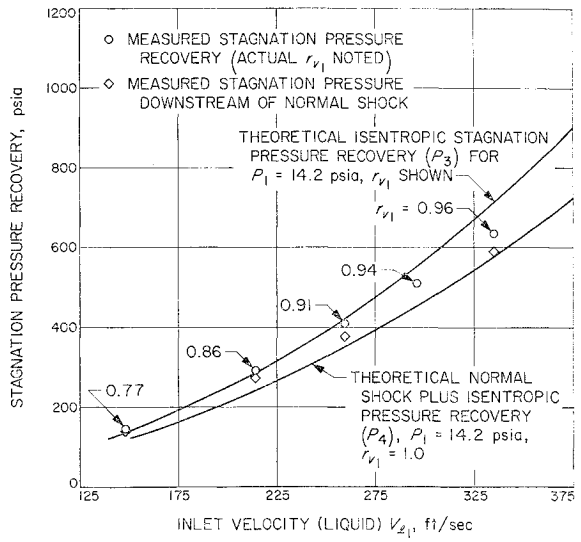

Fig. 18 Stagnation pressures measured both upstream and downstream of a normal shock as a function of liquid velocity at the tunnel volume ratio.

τ_{w_l} or negligible) and 1.0 shows that the simple relationship

$$\tau = (\tau_{w_l}) \text{ (liquid volume fraction)} \tag{24}$$

can be conservatively used for predicting wall shear in high-velocity, homogeneous, two-phase liquid-gas flows.

Equation (24) is equivalent to using the mixture density (ρ = liquid density × liquid volume fraction, ignoring gas density) of the two-phase flow and calculating the shear stress as though the mixture were a single-phase medium. If friction factors for the experiments are computed as a function of mixture density and plotted against Reynolds number also as a function of mixture density and liquid velocity, then the results for the 0.5 volume fraction case fall within 10% of the Prandtl-von Kármán Resistance Law.

8. Summary and Conclusions

Results from the operation of the supersonic, two-phase tunnel indicate that all of the shock phenomena including normal, oblique, and conical shocks that are typical of single-phase, supersonic gas flows can be generated in supersonic, two-phase, gas-liquid continuum type flows. Shock angles, pressure ratios, volume ratios, velocity ratios, and Mach numbers can be accurately predicted by the relatively simple isothermal theory for a two-phase continuum (the two-phases were selected to preclude significant condensation or

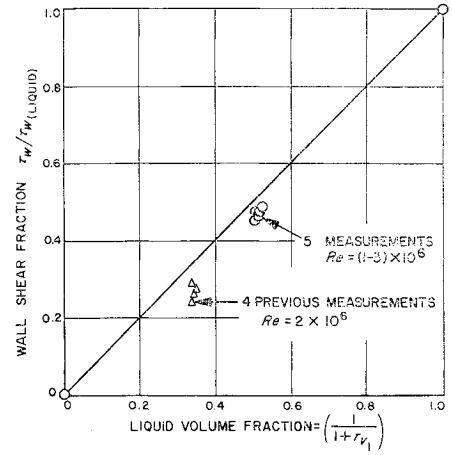

Fig. 19 Variation of wall shear fraction with liquid volume fraction.

dissolution of the gas phase into the liquid phase). Such inherent complexities of the interphase relationships as surface tension, dynamic bubble behavior, heat conduction and dissolution of the gas phase into the liquid phase can be neglected for a wide range of volume ratios and shock strengths as long as the flow characteristics are determined outside of the region in which the various relaxation processes are taking place.

The supersonic, two-phase tunnel is capable of providing uniform, well-defined supersonic flows at Mach numbers from 1 to nearly 100 giving it the most extended Mach number range of any such device in existence. Such uniformity results from the multitube water and gas injector that operated at a fixed area ratio for a wide range of mass-flow rates.

The propagation velocity of a shock wave in a two-phase, liquid-gas continuum corresponds closely to the velocity predicted by the isothermal theory. Such waves have a finite structure that depends upon the gas-liquid volume ratio, isotropy of phase distribution, and wave strength.

The first visible evidence of shock structure occurs at a volume ratio of approximately 0.77 for all mixture velocities. For strong shocks, this evidence is a rapid disorientation of the chain-like bubble structure into a random pattern. Disorientation was less pronounced in the progressively weaker shocks such as the weak oblique shocks, where their presence was evidenced primarily by the change in direction of the bubble chains upon passing through the shock front.

There was no evidence of Prandtl-Meyer type flow around expansion corners in the supersonic, two-phase flow. Although no diffuser work was done in the investigation, it is obvious that expansion without substantial separation can occur only at very limited diffuser angles.

Over-all volume ratio and void fraction distribution for an initially uniform two-phase, liquid-gas flow will continuously change in duct flow because of wall shear stress. The reduced water velocity in the developing boundary layers tends to decrease the core volume ratio and create changing void distributions within the boundary layer. A positive pressure gradient concurrent with the change in volume ratio will cause a deceleration of the gaseous phase in accordance with the interphase drag model. For a gaseous-connected model of relatively low interphase drag, relative velocities can reach a substantial fraction of the flow velocity.

The isentropic stagnation pressure recovery theory for two-phase continuum flows gives a close approximation to the stagnation pressure recovery measured by a total head probe for mixture velocities approaching 270 fps. Above this velocity, the measured pressure drops below the isentropic predicted value and becomes more closely approximated by the normal shock pressure rise, which is followed by an isentropic stagnation recovery of the downstream flow. Here again, the shock thickness in which the relaxation processes are taking place is substantially greater than the distance to the probe opening. Consequently, the relaxation processes have not been completed at the stagnation position.

Results of the investigation into the coefficient of friction indicate that the wall shear stress for two-phase, supersonic flow can be conservatively approximated by multiplying the liquid volume fraction of the mixture by the wall shear stress of a liquid component that flows at the same velocity as the two-phase flow. This relationship is equivalent to using the mixture density ρ of the two-phase flow for calculation of shear stress as though the mixture were a single-phase media. For a more detailed derivation of equations, complete listing of all results and extension of variable relationships through a wide range of Mach numbers, the reader is referred to Ref. 11.

References

[1] Elliott, D. G., "Two Fluid Magnetic Hydrodynamic Cycle for Nuclear-Electric Power Conversion," *ARS Journal*, Vol. 32, No. 6, June 1962, pp. 924–928.

[2] Mallock, A., "The Damping of Sound in Frothy Liquids," *Proceedings of the Royal Society, Series A*, Vol. 84, 1910, pp. 391–395.

[3] Ackeret, J., "Experimental and Theoretical Investigations on Cavitation in Water," *Techmische Mechanik and Thermodynamic (Forschung)*, Vol. 1, No. 1, Berlin, 1930.

[4] Wood, A. B., *A Textbook of Sound*, Macmillan, New York, 1941, p. 361.

[5] Spitzer, L., Jr., "Acoustic Properties of Gas Bubbles in a Liquid," NDRC Rept. 6.1-SR 20-918, PB 31026, OSRD Rept. 1705, July, 1943, National Defense Research Committee.

[6] Campbell, I. J., "Note on Sound Propagation in a Gas-Liquid Mixture," A.R.L./NI/G/H7/17/0, Aug. 1957, Aeronautical Research Council.

[7] Campbell, I. J. and Pitcher, A. S., "Shock Waves in a Liquid Containing Gas Bubbles," *Proceedings of the Royal Society, Series A*, Vol. 243, Feb. 1958, p. 534.

[8] Parkin, B. R., Gilmore, F. R., and Brode, H. L., *Shock Waves in Bubbly Water*, Memo RM-2795-PR, Oct. 1961, RAND Corp., Santa Monica, Calif.

[9] Elliott, D. et al., "Liquid MHD Power Conversion," *Supporting Research and Advanced Development, Space Programs Summary 37-23*, Vol. IV, Oct. 1963, Jet Propulsion Lab., Pasadena, Calif., pp. 132–135.

[10] Muir, J. F. and Eichorn, R., "Compressible Flow of an Air Water Mixture Through a Vertical, Two-Dimensional, Converging-Diverging Nozzle," *Proceedings of 1963 Heat Transfer and Fluid Mechanics Institute*, Stanford University Press, 1963.

[11] Eddington, R. B., *Investigation of Supersonic Shock Phenomena in a Two-Phase (Liquid-Gas) Tunnel*, TR 32-1096, NAS 7-100, March 1967, Jet Propulsion Lab., Pasadena, Calif.